

EDMAE: An Efficient Decoupled Masked Autoencoder for Standard View Identification in Pediatric Echocardiography*

Yiman Liu^{a,b,1}, Xiaoxiang Han^{c,1}, Tongtong Liang^{d,1}, Qiaohong Liu^{e,*}, Qingli Li^{b,*}, Yuqi Zhang^{a,*}

^a*Department of Pediatric Cardiology, Shanghai Children's Medical Center, School of Medicine, Shanghai Jiao Tong University, Shanghai, 200127, China*

^b*Shanghai Key Laboratory of Multidimensional Information Processing, School of Communication & Electronic Engineering, East China Normal University, Shanghai, 200241, China*

^c*School of Health Sciences and Engineering, University of Shanghai for Science and Technology, Shanghai, 200093, China*

^d*Minhang District Centers for Disease Control and Prevention, Shanghai, 201101, China*

^e*School of Medical Instruments, Shanghai University of Medicine and Health Sciences, Shanghai, 201318, China*

Abstract

An efficient decoupled masked autoencoder (EDMAE), which is a novel self-supervised method is proposed for standard view recognition in pediatric echocardiography in this paper. The proposed EDMAE based on the encoder-decoder structure forms a new proxy task. The decoder of EDMAE consists of a teacher encoder and a student encoder, in which the teacher encoder extracts the latent representation of the masked image blocks, while the student encoder extracts the latent representation of the visible image blocks. A loss is calculated between the feature maps output from two encoders to ensure consistency in the latent representations they extracted. EDMAE replaces the VIT structure in the encoder of traditional MAE with pure convolution operation to improve training efficiency. EDMAE is pre-trained in a self-supervised manner on a large-scale private dataset of pediatric echocardiography, and then fine-tuned on the downstream task of standard view recognition. The high classification accuracy is achieved in 27 standard views of pediatric echocardiography. To further validate the effectiveness of the proposed method, another downstream task of cardiac ultrasound segmentation is performed on a public dataset CAMUS. The experiments show that the proposed method not only can surpass some recent supervised methods but also has more competitiveness on different downstream tasks.

Keywords: Self-supervised Learning, Efficient Decoupled Masked Autoencoder, Pediatric Echocardiography, Standard View Identification

1. Introduction

*This project was partially supported by the Natural Science Foundation of China (Grant No.61975056), the Shanghai Natural Science Foundation (Grant No.19ZR1416000), the Shanghai Municipal Health Commission (Project No.20194Y0321) and the Minhang District Public Health Excellent Youth Talent Training Project (Project No.2020FM29).

*Authors are equally corresponded.

Email addresses: LiuyimanSCMC@163.com (Yiman Liu), gtlinyer@163.com (Xiaoxiang Han), zhimaliang@163.com (Tongtong Liang), hq11qh@163.com (Qiaohong Liu), qlli@cs.ecnu.edu.cn (Qingli Li), changyuqi@hotmail.com (Yuqi Zhang)

¹These authors contributed equally to the work.

Congenital heart disease (CHD) is the most common birth defect, with an incidence of 0.9% in live births. It is also the leading cause of death among children aged 0-5 years [1]. In China, approximately 150,000 newborns are diagnosed with CHD annually, and about 120,000 require treatment. If left untreated, one-third of these cases can result in severe complications and death within a year of birth. Thus, early and accurate diagnosis of CHD is crucial.

Transthoracic echocardiography (TTE) is a non-invasive, non-radiation, and low-cost imaging technique that can provide real-time and dynamic observations of the heart. TTE can quickly detect various abnormalities of the heart which becomes an essential tool for the diagnosis and treatment of CHD nowadays [2]. However, the anatomy and spatial configuration of congenital heart disease are complex and variable, and accurate diagnosis through TTE is complicated and time-consuming, requiring experienced cardiac specialists to make accurate judgments on each ultrasound image view.

To ensure accurate and reproducible diagnosis, standard imaging techniques are used for 2D, M-mode, and color Doppler echocardiography [3], meaning that images are obtained in a reproducible manner using the same protocol. This approach is recommended by the American Society of Echocardiography to reduce differences between observers and within observers and to measure specific structures. However, obtaining accurate standard views is a prerequisite for subsequent biometric measurement and final diagnosis of CHD [4].

In China, there is a shortage of experienced cardiac specialists, particularly in rural areas. Therefore, the development of an automatic diagnosis system for congenital heart disease is necessary to address the difficulties in diagnosing CHD at the grassroots level. Such a system could potentially improve the accuracy and efficiency of CHD diagnosis, reduce the burden on specialists, and ultimately improve the prognosis of CHD patients.

With the rapid advancement of artificial intelligence, deep learning has found widespread applications in the field of medicine. One such application is the UNet [5], which is used for medical image segmentation. However, deep learning models require large annotated datasets to accurately fit the target function, and in the medical field, such data annotation is often challenging and expensive. To address this issue, self-supervised learning has gained popularity in recent years, as it reduces the cost of annotating large-scale datasets. This approach leverages custom pseudo-labels to supervise training and uses the learned latent representations for multiple downstream tasks [6]. A powerful self-supervised method in medical image analysis [7, 8, 9, 10, 11] is the mask autoencoder, which has been rapidly applied in recent studies. For example, Zhou et al. [7] applied autoencoders to medical image analysis and verified their efficacy on

multiple medical datasets and tasks. Tian et al. [8] used a memory-enhanced multi-level cross-attention mask autoencoder for unsupervised anomaly detection on medical images, while Xiao et al. [9] conducted extensive research on mask autoencoders for multi-label chest disease classification, achieving advanced performance on chest X-ray images. To adapt to small medical datasets, some researchers [10] have replaced the ViT [12] used by MAE [13] with Swin Transformer [14], while others [11] have applied mask autoencoders to medical multimodal data.

Self-supervised pre-training for images currently relies on learning from degradation, where certain information from the image signal is removed and the algorithm is required to restore it. However, this approach has a bottleneck due to the conflict between degradation strength and semantic consistency. When the degradation is strong enough, it may not guarantee semantic consistency between the image before and after degradation. To address this issue, we propose an efficient decoupled masked autoencoder (EDMAE), which can ensure semantic consistency between images before and after degradation even at high masking rates. The proposed method is based on pure convolutional operations [15], which are lightweight and faster than the ViT used by Masked Autoencoder (MAE) and BEiT [16]. Additionally, we decouple the encoder and decoder to extract more high-quality semantic information since MAE does not fully stimulate the representation learning ability of the encoder. We pre-trained our proposed method on a large-scale unlabeled dataset of pediatric cardiac ultrasound views that we constructed in this study. We then validated the method on a private dataset of pediatric cardiac ultrasound standard views. We also conducted experiments on the public dataset CAMUS to demonstrate that our proposed method can extract effective representations from the pre-trained pediatric cardiac ultrasound dataset.

The main contributions of this paper are as follows.

1. We propose an efficient decoupled masked autoencoder (EDMAE), which is an encoder-decoder structure that includes a teacher encoder and a student encoder. A loss function is used to calculate the loss between the two encoders.
2. The proposed method is pre-trained on a large-scale private dataset of pediatric cardiac ultrasound im-

ages to extract high-quality semantic information. It is then fine-tuned on the downstream task of standard pediatric cardiac ultrasound view recognition. Compared to supervised methods, the proposed self-supervised method is more competitive.

3. The proposed method is validated on another downstream task of cardiac ultrasound segmentation and compared with several mainstream methods. The experimental results demonstrate that the proposed method is more competitive.

2. Related Works

2.1. Self-supervised learning

Self-supervised learning can be categorized into two main types: generative and contrastive. Contrastive learning (CL) is a discriminative method that brings similar samples closer together while pushing different samples farther apart. In 2020, the introduction of MoCo [17] brought contrastive learning to a new stage by using a dynamic dictionary library, avoiding the memory bottleneck problem faced by SimCLR [18]. MoCo achieved accuracy levels close to those obtained through supervised training.

Generative learning is another form of self-supervised learning. Since the introduction of Generative Adversarial Networks (GANs) [19] in 2014, generative models have made significant progress. Recently, Masked Image Modeling (MIM) has become a popular generative self-supervised algorithm with the introduction of MAE, SimMIM [20], and BEiT. These methods learn feature representations by compressing input data into an encoding and then reconstructing the input. Recently, several works have been proposed to improve this method, such as CAE [21] and TACO [22].

2.2. Self-supervised learning in medical image analysis

In the field of medical image analysis, data with high-quality annotations are very scarce. Therefore, self-supervised methods have been quickly introduced in this area. Sowrirajan et al. [23] used the contrastive self-supervised method MoCo for self-supervised pre-training on a chest X-ray dataset, and then fine-tuned on CheXpert with labeled data. They found that self-supervised pre-training on medical datasets was better than supervised

ImageNet pre-trained models. Navarro et al. [24]’s work showed that self-supervised methods outperform previous supervised algorithms in multi-organ segmentation tasks.

Additionally, generative self-supervised algorithms have been proposed for medical image analysis. Ly et al. [25] proposed the Double Loss Adaptive Masked Autoencoder (DAMA) for multi-immunofluorescence brain image analysis, and their method achieved excellent results on multiple tasks. Quan et al. [26] proposed a Global Contrastive Masked Autoencoder for processing pathological images, which achieved competitive results compared to other methods. Furthermore, there are many new research findings [7, 8, 9, 10, 11].

2.3. Autoencoder

Autoencoder (AE) is an self-supervised learning algorithm that learns representations of input information by using the input itself as the learning target [27]. Classic autoencoders include PCA and k-means [28]. Since the introduction of Masked Autoencoder (MAE) and BEiT in 2021, autoencoders have become increasingly popular in computer vision self-supervised learning. Recently, they have been increasingly applied in medical image analysis [9, 25, 26, 29].

3. Proposed Method

3.1. Masked Autoencoder

The MAE algorithm employs a random masking technique to obscure certain patches of the input image, which it then reconstructs by filling in the missing pixels. This approach is based on two fundamental design principles: (1) an asymmetric encoder-decoder architecture that handles visible patches differently than mask tokens. The encoder encodes only visible patches and disregards mask tokens, whereas the decoder utilizes the encoder’s output (i.e., a latent representation) and mask tokens to reconstruct the image. (2) Using a higher mask ratio has demonstrated promising outcomes. Specifically, a mask rate of 75% has been shown to produce favorable results.

The MAE algorithm operates through a series of steps. Initially, it segments the input image into patches and applies a masking operation to them. Subsequently, it feeds the visible patches into the encoder along with the mask tokens. The encoder’s output, as well as the mask tokens,

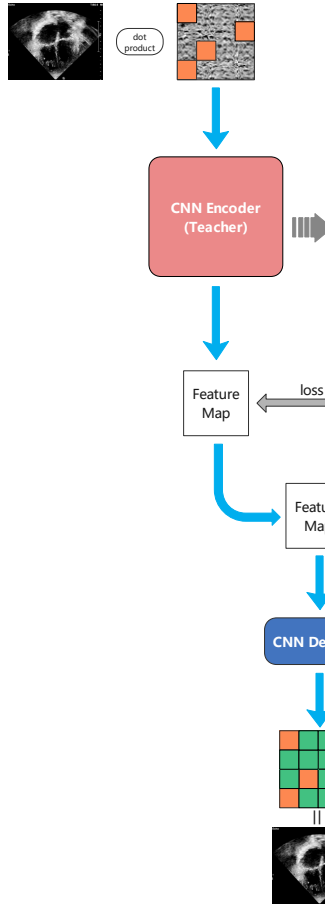


Figure 1: The overall architecture of EDMAE.

serve as input to the lightweight decoder, which reconstructs the entire image. The mean squared error (MSE) loss function is employed, and it is only computed for the masked patches. MAE has exhibited strong transferability, achieving an impressive accuracy of 87.8% on the ImageNet-1K dataset. Furthermore, its simplicity enables it to scale up and become a promising option for large-scale image processing applications.

3.2. Overall structure of EDMAE

The proposed method consists of two inputs, namely the visible and invisible parts of the input image. A convolutional neural network in a proxy task predicts the invisible part from the visible part, forcing the encoder to

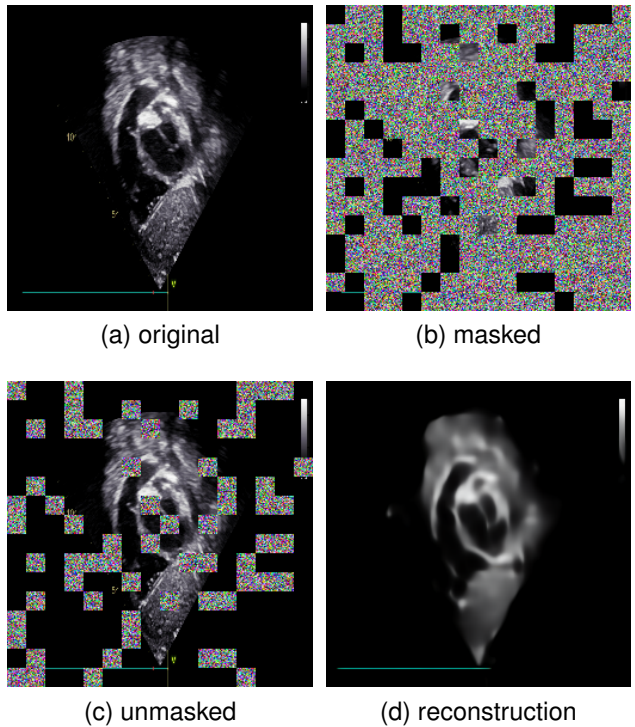


Figure 2: The original image, the image masked by 75%, the unmasked part of the image, and the reconstructed image.

learn the latent representation of the image. The proposed method uses two encoders with convolutional neural networks called DenseNet [15]. One encoder is updated through backpropagation and is called the teacher encoder, while the other encoder's backpropagation is blocked and cannot update its weights. It is called the student encoder, which shares weights with the teacher encoder. The decoder and encoder use the same network to predict masked image blocks. The proposed method computes losses in two places, one is between the feature maps output by the two encoders, and the other is between the reconstructed image output by the decoder and the original image.

3.3. Self-supervised pretraining

The proposed self-supervised pretraining method is formally an optimization problem, which is a task of solving static linear inverse problems through a deep neural net-

work. $z \in \mathbb{R}^L$ serves as input, and by optimizing the parameters θ of the untrained neural network f_θ , it generates an output $f_\theta(z)$ that is consistent with the measurement values $y \in \mathbb{R}^M$.

$$\theta^* = \underset{\theta}{\operatorname{argmin}} \|y - F(f_\theta(z))\|_2^2 \quad (1)$$

where $F \in \mathbb{R}^{M \times N}$ is the forward model. In this paper, y is the masked image, and F is the masking operation. The output of the optimized network $x^* = f_{\theta^*}(z)$ produces remarkably high-quality reconstructed images.

The proposed self-supervised training method follows the workflow described below. Initially, visible image blocks are fed into the encoder to extract their representations. Next, predictions are made in the encoding representation space, ensuring that the masked image blocks' representations are consistent with those predicted from the visible image blocks. Finally, the decoder takes in the representations of the masked image blocks to predict the masked image blocks. Since previous research [13] has shown that a 75% masking rate produces optimal representations in autoencoders, this paper will use a 75% masking rate by default. As shown in Fig.2., the original image, the image masked by 75%, the unmasked part of the image, and the reconstructed image are shown in the figure.

The loss calculated between the feature maps output by the two encoders is called feature alignment. The advantage of this approach is that it can ensure that the representation of the mask image block is consistent with the representation obtained from the prediction of the visible image block, ensuring that the image before and after degradation has semantic consistency. It can be represented by the following expression:

$$y_1 = F(x_m) \quad (2)$$

$$y_2 = F^*(x_{um}) \quad (3)$$

$$\text{loss} = \text{MSE}(y_1, y_2) \quad (4)$$

Among them, x_m represents the masked image, x_{um} represents the unmasked image, and MSE represents the mean squared error loss function (MSE Loss, L2 Loss).

3.4. Downstream task

After completing self-supervised pre-training, all that is needed is to replace the decoder of the proposed method with a task-specific head that caters to the downstream task's characteristics.

For the task of standard view recognition in pediatric cardiac ultrasound, the labels consist of multiple fixed categories, making it an image classification task. Therefore, the decoder needs to be replaced with a linear layer, and cross-entropy is used as the loss function to fine-tune the entire network.

For the task of cardiac ultrasound segmentation, a segmentation task head is required. In this paper, we use the decoder of our own implementation of DenseUNet as the segmentation head. Specifically, the feature maps output by the encoder are used as the input to the segmentation task head, which outputs the segmentation results. The Focal loss is used to compute the loss between the segmentation results and the ground truth labels.

4. Experiment

4.1. Dataset

Our dataset is divided into a private dataset of children's cardiac ultrasound views and a public dataset CAMUS [30]. The private children's cardiac ultrasound view data is divided into two parts, one of which has 17,755 unlabeled children's cardiac ultrasound view data for self-supervised pre-training. The other part is the labeled children's echocardiography standard view data with 1026 images for fine-tuning. The data used for fine-tuning includes 616 training sets, 205 validation sets and 205 test sets, which cover 27 standard views of children's echocardiography, 1 other blood flow spectrum and 1 other views. The CAMUS dataset contains two-chamber and four-chamber acquisitions from 500 patients, as well as reference measurements from one cardiologist for the full dataset and three cardiologists for 50 patients.

4.2. Training Details

We designed our model based on the machine learning framework PyTorch1.12.1 using Python3.8. In particular, we also use PyTorch-Lightning1.6.5, an efficient and convenient framework based on PyTorch. In addition, some

Table 1: Comparative Experiments on Private Datasets.

Method	Overall Accuracy (%)	Mean Precision (%)	Mean Recall (%)	Mean Specificity (%)	Mean F1 (%)
mobileNetV3-L	99.17	89.68	90.10	99.57	89.06
ResNet50	99.34	91.80	92.30	99.65	91.58
Swin-T-B	99.35	92.12	92.46	99.65	91.68
DenseNet121	99.35	92.29	92.66	99.66	91.73
ours	98.48	93.20	94.62	99.73	93.63

of our comparison experiments and ablation experiments use the backbone network provided in Torchvision0.13.1.

We trained the proposed model on a GPU server with an Intel Core i9-10900X CPU, two 10GB Nvidia RTX3080 GPUs, 32GB RAM, and 20GB VRAM.

We set the batch size of data according to different networks to ensure maximum memory utilization. The number of threads of the data reading program is 16. The initial learning rate is 1e-3. The learning rate dynamic adjustment strategy is ReduceLROnPlateau. The optimizer is AdamW [31]. The training epoch number is 100. Train with automatic mixed precision.

The loss function used for pre-training is the mean square error (MSE) loss function. The loss function for downstream classification tasks is the cross-entropy loss function. The loss function for downstream segmentation tasks is Focal Loss [32], which can reduce the weight of easily classified samples and increase the weight of difficult-to-classify samples. Its formula is as follows:

$$FL(p_t) = -\alpha_t(1 - p_t)^\gamma \log(p_t) \quad (5)$$

$p \in [0,1]$ is the model's estimated probability of the labeled class, γ is an adjustable focusing parameter, and α is a balancing parameter. We set γ to 2 and α to 0.25.

4.3. Evaluation Metrics

To evaluate the performance of the proposed EDMAE, we use some commonly used metrics to assess the accuracy of the model. For classification tasks, we use Overall Accuracy (OA), Precision, Recall, Specificity, and F1-Score (F1). These evaluation metrics are calculated based on a confusion matrix, where TP represents the number of True Positive samples, TN represents the number of True

Negative samples, FP represents the number of False Positive samples, and FN represents the number of False Negative samples.

Overall Accuracy (OA) is used to measure the overall accuracy of the model's predicted results:

$$OA = \frac{TP + TN}{TP + TN + FP + FN} \quad (6)$$

F1 Score represents a comprehensive consideration of Precision and Recall:

$$Precision = \frac{TP}{TP + FP} \quad (7)$$

$$Specificity = \frac{TN}{FP + TN} \quad (8)$$

$$Recall = \frac{TP}{TP + FN} \quad (9)$$

$$F1 = 2 \frac{Precision \times Recall}{Precision + Recall} = \frac{2TP}{2TP + FP + FN} \quad (10)$$

For the task of cardiac ultrasound segmentation, we adopt three metrics: Dice coefficient (DC), Hausdorff distance (HD), and area under the curve (AUC).

$$DC = \frac{2 \times |A \cap B|}{|A| + |B|} = \frac{2TP}{2TP + FN + FP} \quad (11)$$

$$HD = \max \{d_{AB}, d_{BA}\} \\ = \max \{\max_{a \in A} \min_{b \in B} d_{(a,b)}, \max_{b \in B} \min_{a \in A} d_{(a,b)}\} \quad (12)$$

4.4. Experimental results on the private dataset

The advantages of the proposed method were validated on a private dataset constructed in this study. The proposed method was compared with several mainstream classification networks, including MobileNetV3-Large,

Table 2: Experimental results on the private dataset (the **blue** value represents the best value in this column, and the **red** value represents the worst value in this column).

Standard View	Accuracy (%)	Precision (%)	Recall (%)	Specificity (%)	F1 (%)
LPS5C	99.74	99.99	91.66	99.99	95.45
PSPA	99.22	85.00	95.00	99.46	89.44
PSAX	99.74	94.44	99.99	99.73	97.06
subCE	99.74	90.00	99.99	99.73	94.44
subIVC	98.18	81.66	78.03	99.18	79.76
sub4C	99.99	99.99	99.99	99.99	99.99
sub5C	99.99	99.99	99.99	99.99	99.99
subSAS	99.99	99.99	99.99	99.99	99.99
subRVOT	99.99	99.98	99.98	99.99	99.98
A4C	99.74	93.75	99.99	99.73	96.66
A5C	99.99	99.99	99.99	99.99	99.99
LPS4C	99.74	92.85	99.99	99.73	96.15
sax-mid	99.22	93.74	88.88	99.73	91.17
PSLV	99.22	80.91	99.99	99.19	89.44
supAO	99.99	99.99	99.99	99.99	99.99
Others	96.87	87.08	77.29	98.85	81.82
M-AO	99.99	99.99	99.99	99.99	99.99
M-LV	99.99	99.99	99.99	99.99	99.99
M-TV	99.99	99.99	99.99	99.99	99.99
DP-ABAO	99.99	99.99	99.99	99.99	99.99
DP-MV	99.48	92.85	92.85	99.73	92.85
DP-TV	99.22	93.75	86.60	99.73	89.90
DP-AAO	99.48	91.66	91.66	99.73	91.66
DP-PV	99.22	87.50	92.85	99.46	90.00
DP-DAO	98.96	76.19	90.00	99.20	82.51
DP-TDI	99.99	99.99	99.99	99.99	99.99
DP-PVR	99.48	87.49	89.99	99.74	87.30
DP-TVR	99.74	87.50	99.99	99.74	92.85
DP-OTHER	97.92	86.60	69.32	99.45	76.84
Mean	99.48	93.20	94.62	99.73	93.63

ResNet50, Swin-Transformer-Base, and DenseNet121. These networks are all from the PyTorchVision built-in model module and have loaded pre-trained weights of ImageNet-1k. As shown in Table1, the proposed method outperformed other models in all metrics, with an average F1 score 2.45% higher than DenseNet121.

Our dataset consists of 29 categories, which include low parasternal five-chamber view (LPS5C), parasternal view of the pulmonary artery (PSPA), parasternal

short-axis view (PSAX), parasternal short-axis view at the level of the mitral valve (short axis at mid, sax-mid), parasternal long-axis view of the left ventricle (PSLV), suprasternal long-axis view of the entire aortic arch (supAO), Long axis view of subcostal inferior vena cava (subIVC), subcostal four-chamber view (sub4C), subcostal five-chamber view (sub5C), subcostal sagittal view of the atrium septum (subSAS), subcostal short-axis view through the right ventricular outflow tract (subRVOT),

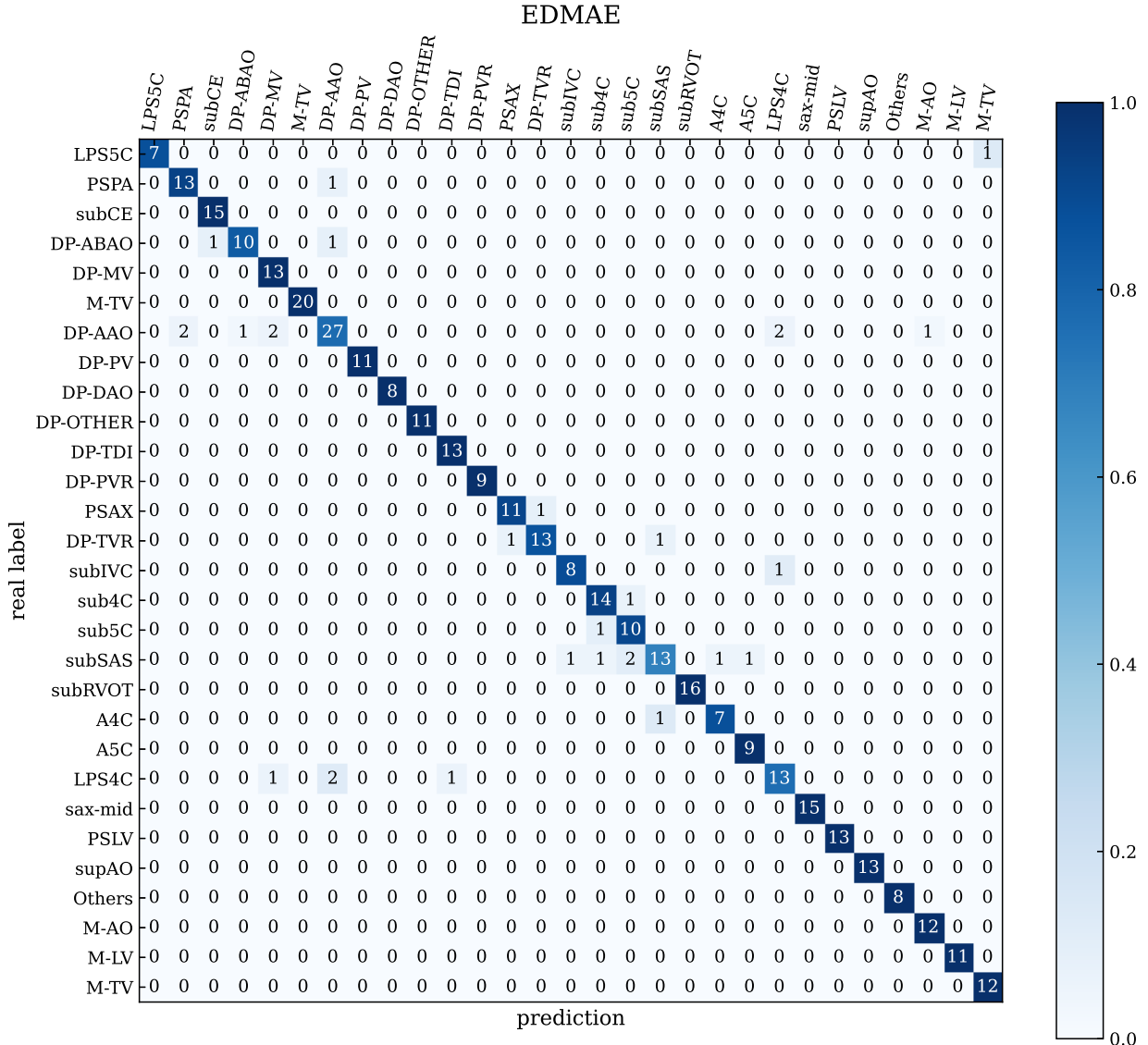


Figure 3: The confusion matrix of the test results of the proposed method on a private dataset.

apical four-chamber view (A4C), apical five-chamber view (A5C), low parasternal four-chamber view (LPS4C), subxiphoid cat's eye view (subCE), other views (others), M-mode echocardiographic recording of the aortic (M-AO), M-mode echocardiography recording of the left ventricle(M-LV), M-mode echocardiography recording of

the tricuspid valve (M-TV), Doppler recording from the abdominal aorta (DP-ABAO), Doppler recording from the mitral valve (DP-MV), Doppler recording from the tricuspid valve (DP-MV), Doppler recording from the ascending aorta (DP-AAO), Doppler recording from the pulmonary valve (DP-PV), Doppler recording from the de-

Table 3: Experimental results on the public dataset CAMUS.

Method	DC (%)	HD (mm)	AUC (%)
Joint-net	91.05 ± 0.27	3.41 ± 0.86	97.14 ± 0.25
DenseUNet	91.88 ± 0.26	3.34 ± 0.82	97.26 ± 0.24
TransUNet	91.89 ± 0.38	3.25 ± 1.01	97.39 ± 0.24
MFP-Net	92.23 ± 0.29	3.40 ± 0.97	97.28 ± 0.23
PLANet	92.61 ± 0.40	3.10 ± 0.93	97.58 ± 0.23
ours	93.09 ± 0.22	3.02 ± 0.81	97.84 ± 0.22

scending aorta (DP-DAO), Doppler recording from the tissue doppler imaging (DP-TDI), other Doppler recordings (DP-OTHER), Doppler recording from the pulmonary valve regurgitation (DP-PVR), Doppler recording from the tricuspid valve regurgitation (DP-TVR) and Doppler recording from the tricuspid valve regurgitation (DP-TV). As can be seen from Table 2 and Fig.3., the proposed method performs well in classifying most of the views, especially for sub4C, sub5C, and subSAS, which have the best recognition results. However, the recognition performance for other views and DP-OTHER is poor.

4.5. Experimental results on the public dataset CAMUS

To further demonstrate the superiority of the proposed method, a comparison was made with five other methods on the public dataset CAMUS, including MFP-Net [33], Joint-net [34], TransUNet [35], PLANet [36], and DenseUNet implemented by ourselves. As shown in Table 3, the proposed method outperformed other models in all metrics, with a DC 0.39% higher than the advanced PLANet and lower HD.

As shown in Fig.4., we compared the segmentation results of our proposed method with those of other methods. Our proposed method can achieve good segmentation results on ultrasound images of multiple scales. DenseUNet’s segmentation performance is poor, with uneven segmentation edges in large-scale object segmentation and unsatisfactory segmentation results for small-scale objects. However, our DenseUNet model, which underwent self-supervised pretraining, performs much better in segmentation compared to the DenseUNet model without self-supervised pretraining.

5. Discussion

EDMAE achieved excellent classification and segmentation performance through self-supervised pre-training on a large-scale dataset of pediatric cardiac ultrasound. From the experiments described above, it can be seen that the proposed method has significant advantages over other methods in downstream tasks such as pediatric cardiac standard view recognition, with good recognition performance for most views and only poor recognition for views with less distinct features. In addition, the proposed method performs well on the public dataset CAMUS and outperforms many advanced methods, showing good performance for object segmentation at multiple scales.

There are three primary factors contributing to the outstanding performance of EDMAE. Firstly, the self-supervised pre-training data distribution is similar to that of downstream tasks, allowing models trained on large-scale data to effectively learn the data distribution. Secondly, the encoder of EDMAE is decoupled from the decoder, which compels the encoder to completely extract the latent semantic representation. Finally, the alignment operation of EDMAE guarantees semantic consistency between the images before and after degradation.

6. Conclusion

In this paper, an efficient decoupled masked autoencoder with the strong feature extraction ability is proposed for standard view recognition on pediatric echocardiography. The model pre-trained on a private large-scale children’s cardiac ultrasound dataset has shown excellent performance in the downstream task of children’s heart standard view recognition, which surpasses some advanced classification methods. The proposed model also can be

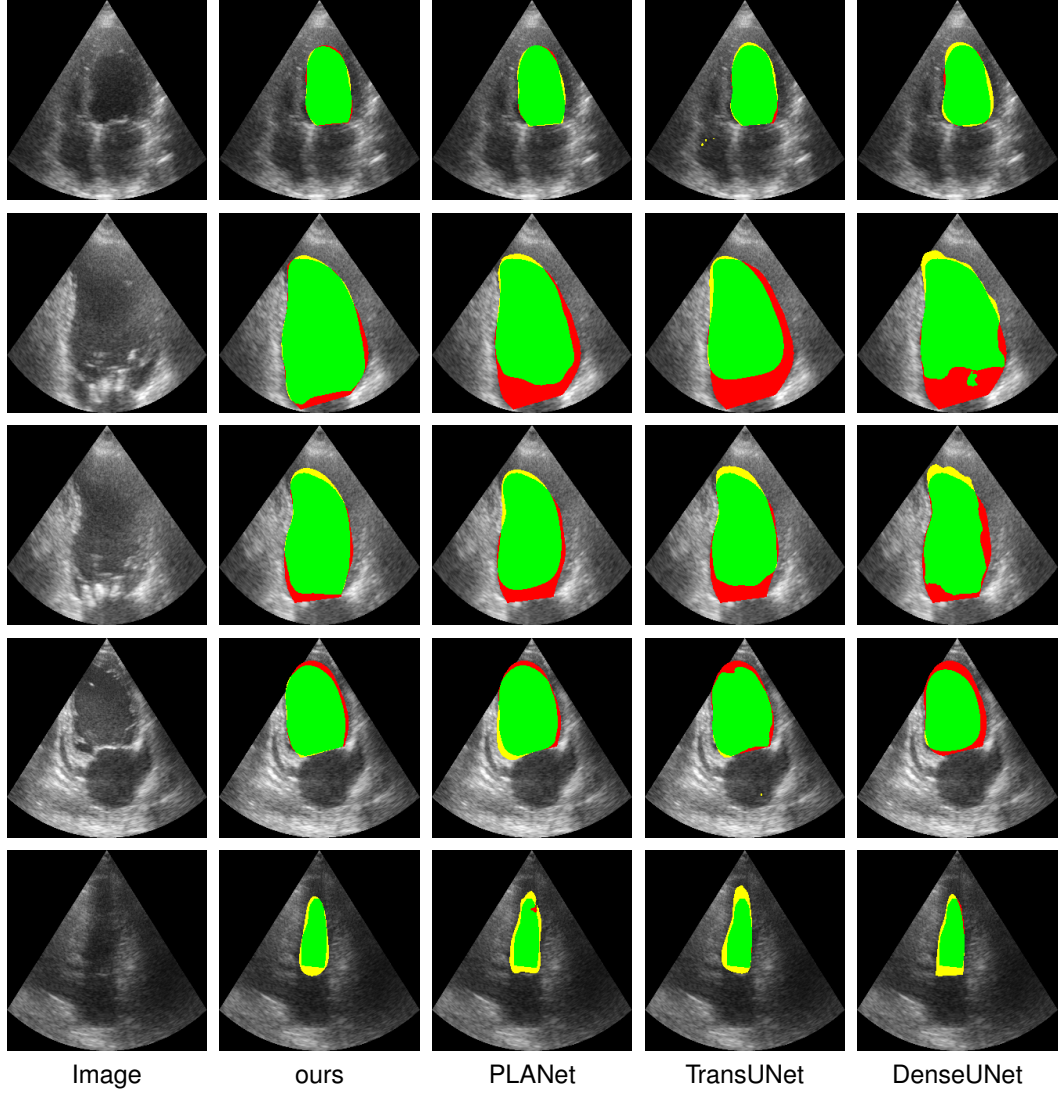


Figure 4: Experimental results on the public dataset CAMUS. The green area represents the overlapping part between the prediction and ground truth, the red area represents the part of ground truth not covered by the prediction, and the yellow area represents the part of the prediction that goes beyond the ground truth.

applied in another downstream task, i.e., cardiac ultrasound segmentation, which achieves good segmentation performance. Since the training images are collected from clinical examination database, the proposed method with the high recognition rate for standard view recognition can provide a good technical basis for intelligent diag-

nosis of congenital heart disease. It would become a new standardized training method for primary-level cardiac ultrasound physicians to practice cardiac view scanning.

References

[1] Q.-M. Zhao, F. Liu, L. Wu, X.-J. Ma, C. Niu, G.-Y. Huang, Prevalence of congenital heart disease at live birth in china, *The Journal of pediatrics* 204 (2019) 53–58.

[2] P. S. Douglas, M. J. Garcia, D. E. Haines, W. W. Lai, W. J. Manning, A. R. Patel, M. H. Picard, D. M. Polk, M. Ragosta, R. P. Ward, et al., Accf/ase/aha/asnc/hfsa/hrs/scai/sccm/scct/scmr 2011 appropriate use criteria for echocardiography: a report of the american college of cardiology foundation appropriate use criteria task force, american society of echocardiography, american heart association, american society of nuclear cardiology, heart failure society of america, heart rhythm society, society for cardiovascular angiography and interventions, society of critical care medicine, society of cardiovascular computed tomography, and society for cardiovascular magnetic resonance endorsed by the american college of chest physicians, *Journal of the American College of Cardiology* 57 (9) (2011) 1126–1166.

[3] L. Lopez, S. D. Colan, P. C. Frommelt, G. J. Ensing, K. Kendall, A. K. Younoszai, W. W. Lai, T. Geva, Recommendations for quantification methods during the performance of a pediatric echocardiogram: a report from the pediatric measurements writing group of the american society of echocardiography pediatric and congenital heart disease council, *Journal of the American Society of Echocardiography* 23 (5) (2010) 465–495.

[4] X. P. Burgos-Artizzu, D. Coronado-Gutiérrez, B. Valenzuela-Alcaraz, E. Bonet-Carne, E. Eixarch, F. Crispí, E. Gratacós, Evaluation of deep convolutional neural networks for automatic classification of common maternal fetal ultrasound planes, *Scientific Reports* 10 (1) (2020) 1–12.

[5] O. Ronneberger, P. Fischer, T. Brox, U-net: Convolutional networks for biomedical image segmentation, in: *Medical Image Computing and Computer-Assisted Intervention–MICCAI 2015: 18th International Conference*, Munich, Germany, October 5-9, 2015, Proceedings, Part III 18, Springer, 2015, pp. 234–241.

[6] A. Jaiswal, A. R. Babu, M. Z. Zadeh, D. Banerjee, F. Makedon, A survey on contrastive self-supervised learning, *Technologies* 9 (1) (2020) 2.

[7] L. Zhou, H. Liu, J. Bae, J. He, D. Samaras, P. Prasanna, Self pre-training with masked autoencoders for medical image analysis, *arXiv preprint arXiv:2203.05573* (2022).

[8] Y. Tian, G. Pang, Y. Liu, C. Wang, Y. Chen, F. Liu, R. Singh, J. W. Verjans, G. Carneiro, Unsupervised anomaly detection in medical images with a memory-augmented multi-level cross-attentional masked autoencoder, *arXiv preprint arXiv:2203.11725* (2022).

[9] J. Xiao, Y. Bai, A. Yuille, Z. Zhou, Delving into masked autoencoders for multi-label thorax disease classification, in: *Proceedings of the IEEE/CVF Winter Conference on Applications of Computer Vision*, 2023, pp. 3588–3600.

[10] Z. Xu, Y. Dai, F. Liu, W. Chen, Y. Liu, L. Shi, S. Liu, Y. Zhou, Swin mae: Masked autoencoders for small datasets, *arXiv preprint arXiv:2212.13805* (2022).

[11] Z. Chen, Y. Du, J. Hu, Y. Liu, G. Li, X. Wan, T.-H. Chang, Multi-modal masked autoencoders for medical vision-and-language pre-training, in: *Medical Image Computing and Computer Assisted Intervention–MICCAI 2022: 25th International Conference*, Singapore, September 18–22, 2022, Proceedings, Part V, Springer, 2022, pp. 679–689.

[12] A. Dosovitskiy, L. Beyer, A. Kolesnikov, D. Weissenborn, X. Zhai, T. Unterthiner, M. Dehghani, M. Minderer, G. Heigold, S. Gelly, et al., An image is worth 16x16 words: Transformers for image recognition at scale, *arXiv preprint arXiv:2010.11929* (2020).

[13] K. He, X. Chen, S. Xie, Y. Li, P. Dollár, R. Girshick, Masked autoencoders are scalable vision learners, in: *Proceedings of the IEEE/CVF Conference on Computer Vision and Pattern Recognition*, 2022, pp. 16000–16009.

[14] Z. Liu, Y. Lin, Y. Cao, H. Hu, Y. Wei, Z. Zhang, S. Lin, B. Guo, Swin transformer: Hierarchical vision transformer using shifted windows, in: Proceedings of the IEEE/CVF international conference on computer vision, 2021, pp. 10012–10022.

[15] G. Huang, Z. Liu, L. Van Der Maaten, K. Q. Weinberger, Densely connected convolutional networks, in: Proceedings of the IEEE conference on computer vision and pattern recognition, 2017, pp. 4700–4708.

[16] H. Bao, L. Dong, S. Piao, F. Wei, Beit: Bert pre-training of image transformers, arXiv preprint arXiv:2106.08254 (2021).

[17] K. He, H. Fan, Y. Wu, S. Xie, R. Girshick, Momentum contrast for unsupervised visual representation learning, in: Proceedings of the IEEE/CVF conference on computer vision and pattern recognition, 2020, pp. 9729–9738.

[18] T. Chen, S. Kornblith, M. Norouzi, G. Hinton, A simple framework for contrastive learning of visual representations, in: International conference on machine learning, PMLR, 2020, pp. 1597–1607.

[19] I. Goodfellow, J. Pouget-Abadie, M. Mirza, B. Xu, D. Warde-Farley, S. Ozair, A. Courville, Y. Bengio, Generative adversarial networks, Communications of the ACM 63 (11) (2020) 139–144.

[20] Z. Xie, Z. Zhang, Y. Cao, Y. Lin, J. Bao, Z. Yao, Q. Dai, H. S. Hu, A simple framework for masked image modeling. arxiv 2021, arXiv preprint arXiv:2111.09886.

[21] X. Chen, M. Ding, X. Wang, Y. Xin, S. Mo, Y. Wang, S. Han, P. Luo, G. Zeng, J. Wang, Context autoencoder for self-supervised representation learning, arXiv preprint arXiv:2202.03026 (2022).

[22] Z. Fu, W. Zhou, J. Xu, H. Zhou, L. Li, Contextual representation learning beyond masked language modeling, arXiv preprint arXiv:2204.04163 (2022).

[23] H. Sowrirajan, J. Yang, A. Y. Ng, P. Rajpurkar, Moco pretraining improves representation and transferability of chest x-ray models, in: Medical Imaging with Deep Learning, PMLR, 2021, pp. 728–744.

[24] F. Navarro, C. Watanabe, S. Shit, A. Sekuboyina, J. C. Peeken, S. E. Combs, B. H. Menze, Self-supervised pretext tasks in model robustness & generalizability: A revisit from medical imaging perspective, in: 2022 44th Annual International Conference of the IEEE Engineering in Medicine & Biology Society (EMBC), IEEE, 2022, pp. 5074–5079.

[25] S. T. Ly, B. Lin, H. Q. Vo, D. Maric, B. Roysam, H. V. Nguyen, Student collaboration improves self-supervised learning: Dual-loss adaptive masked autoencoder for brain cell image analysis, arXiv preprint arXiv:2205.05194 (2022).

[26] H. Quan, X. Li, W. Chen, M. Zou, R. Yang, T. Zheng, R. Qi, X. Gao, X. Cui, Global contrast masked autoencoders are powerful pathological representation learners, arXiv preprint arXiv:2205.09048 (2022).

[27] Y. Bengio, A. Courville, P. Vincent, Representation learning: A review and new perspectives, IEEE transactions on pattern analysis and machine intelligence 35 (8) (2013) 1798–1828.

[28] G. E. Hinton, R. Zemel, Autoencoders, minimum description length and helmholtz free energy, Advances in neural information processing systems 6 (1993).

[29] J. Jiang, N. Tyagi, K. Tringale, C. Crane, H. Veeraraghavan, Self-supervised 3d anatomy segmentation using self-distilled masked image transformer (smit), in: Medical Image Computing and Computer Assisted Intervention–MICCAI 2022: 25th International Conference, Singapore, September 18–22, 2022, Proceedings, Part IV, Springer, 2022, pp. 556–566.

[30] S. Leclerc, E. Smistad, J. Pedrosa, A. Østvik, F. Cervenansky, F. Espinosa, T. Espeland, E. A. R. Berg, P.-M. Jodoin, T. Grenier, et al., Deep learning for segmentation using an open large-scale dataset in

2d echocardiography, IEEE transactions on medical imaging 38 (9) (2019) 2198–2210.

- [31] I. Loshchilov, F. Hutter, Fixing weight decay regularization in adam (2017).
- [32] T.-Y. Lin, P. Goyal, R. Girshick, K. He, P. Dollár, Focal loss for dense object detection, in: Proceedings of the IEEE international conference on computer vision, 2017, pp. 2980–2988.
- [33] S. Moradi, M. G. Oghli, A. Alizadehasl, I. Shiri, N. Oveisí, M. Oveisí, M. Maleki, J. Dhooge, Mfp-unet: A novel deep learning based approach for left ventricle segmentation in echocardiography, Physica Medica 67 (2019) 58–69.
- [34] K. Ta, S. S. Ahn, J. C. Stendahl, A. J. Sinusas, J. S. Duncan, A semi-supervised joint network for simultaneous left ventricular motion tracking and segmentation in 4d echocardiography, in: Medical Image Computing and Computer Assisted Intervention–MICCAI 2020: 23rd International Conference, Lima, Peru, October 4–8, 2020, Proceedings, Part VI 23, Springer, 2020, pp. 468–477.
- [35] J. Chen, Y. Lu, Q. Yu, X. Luo, E. Adeli, Y. Wang, L. Lu, A. L. Yuille, Y. Zhou, Transunet: Transformers make strong encoders for medical image segmentation, arXiv preprint arXiv:2102.04306 (2021).
- [36] F. Liu, K. Wang, D. Liu, X. Yang, J. Tian, Deep pyramid local attention neural network for cardiac structure segmentation in two-dimensional echocardiography, Medical Image Analysis 67 (2021) 101873.